Desalination and Water Treatment
www.deswater.com

doi: 10.5004/dwt.2017.20690

76 (2017) 254–264
May

Biotemplated fabrication of hierarchically γ-AlO(OH)/CuMgAl-LDH for removal of Congo red

Chaochao Xu, Jia Li*, Hongyan Li, Min Zuo, Peng Song

School of Material Science and Engineering, University of Jinan, Jinan 250022, PR China, Tel. +86 18766127412, email: mse_xucc@163.com (C. Xu), Tel. +86 13953185430, email: mse_lij@ujn.edu.cn (J. Li), Tel. +86 15106950518, email: 815754663@ujn.edu.cn (H. Li), Tel. +86 15552595131, email: mse_zuom@ujn.edu.cn (M. Zuo), Tel. +8615726120371, email: mse_Songp@ujn.edu.cn (P. Song)

Received 25 August 2016; Accepted 7 March 2017

ABSTRACT

Hierarchically porous γ-AlO(OH)/CuMgAl-LDH with high specific surface area and superior adsorption performance toward Congo Red (CR) were successfully synthesized by combining the biotemplated and hydrothermal method. Hexagonal CuMgAl-LDH nanosheets and honeycombed γ-AlO(OH) nanosheets interwove into 3D hierarchically porous structure through in-situ growths onto the surface of hollow Al_2O_3 fibers that were made from kapok template. The effects of various limiting factors including contact time, pH value and initial concentrate of CR on the adsorption capacity were investigated. γ-AlO(OH)/CuMgAl-LDH synthesized under the hydrothermal temperature of 160°C had the maximum monolayer adsorption capacity of 155.76 mg g^{-1}, which was attributed to the higher BET surface area and 3D hierarchically porous structure. It was found that the CR adsorption by γ-AlO(OH)/CuMgAl-LDH was spontaneous and exothermic and the adsorption process was well fitted with the Langmuir isotherm model and the pseudo second order kinetics model.

Keywords: Biotemplate; γ-AlO(OH); Layered double hydroxides; Congo red; Adsorption

1. Introduction

With the development of the society, the demand of dye increases in many areas, such as textiles, plastics, paper and leather dyeing industries. It is important to note that 10–15% of the dyes release into the environment during the processes of production and use. For the feature of carcinogenicity [1], stabilization and degradation-resistant, the emission of dye wastewater poses a great threat to the health of humans and other organisms. Therefore, the removal of dye has become a very serious and urgent problem. Physical, chemical and biological methods have been applied into the treatment of dye wastewater. Among them, it is worth mentioning that adsorption treatment is well recognized by people because of the high affinity for numerous species of organic dyes. Most importantly, it will not bring other by-products in the adsorption process.

In recent years, the exploration of hierarchical structure materials, which are combined by nanoparticles, nano fiber, nanobelts and so on, has become a research hotspot. Hierarchical structure not only has the characteristic of nanostructure unit, but also has more excellent overall collaborative properties, which can enrich the performance of nano materials. Hierarchical γ-AlO(OH) (known as boehmite) is widely used as adsorbents [2,3], catalyst supports [4,5], pharmaceutical carriers [6], etc. Previous researchers have studied the preparation of hierarchical aluminum hydroxide with various structures, such as flower-like [7], hollow microspheres [8] and urchin-like hollow ball [9] and so on. Therefore it motivates us to fabricate 3D hierarchical materials with γ-AlO(OH) and hydrotalcite-like, which have been considered to be preferable materials as adsorbent for the special properties and unique pore structure [10,11]. Hydrotalcite-like (Layered Double Hydroxides, abbreviated LDH) is a hydrotalcite compound derived. Hydrotalcite-like structure can be expressed as

*Corresponding author.

$$[M^{2+}_{1-x}M^{3+}_{x}(OH)_2]^{x+}[A_{x/n}]^{n-}\cdot mH_2O \quad (1)$$

where M^{2+} and M^{3+} are divalent and trivalent metal cations, respectively. Intermolecular forces existed between object anions and laminate molecules. Certain anions with specific function (e.g. anionic dye molecules of wastewater) can be introduced into the LDH layers through these intermolecular forces, achieving adsorptive separation of organic pollutants. However, extremely limited interlayer space restricts their practical application. One effective solution is to design a structure of multi-dimensional micro-nano composites based on LDH nanosheets and micron-sized structural units.

In recent years, biotemplated method has been regarded as one of the most direct and effective ways to synthesize special materials with controlled morphology, structure and unique properties. So far, there have been a lot of biological materials used as templates, such as microorganisms [12], yeast [13,14], pollen [15,16], kapok [17], protein [18], carbohydrates [19] and butterfly wings [20] and so on. In the biological templated method, the target materials are obtained by the transcription of multi-level hierarchical structures with micropores, mesopores and macro-pore, showing a tempting prospect on adsorption separation technology. In this study, with the advantage of hollow structure of kapok, γ-AlO(OH) and CuMgAl-LDH were assembled into 3D hierarchical structure by biological template, forming hierarchically porous γ-AlO(OH)/CuMgAl-LDH adsorbent. The adsorption performance of γ-AlO(OH)/CuMgAl-LDH was studied by the removal of CR from aqueous solution.

2. Materials and methods

2.1. Materials

Aluminum nitrate nonahydrate (≥99.0%, $Al_3NO_3\cdot 9H_2O$) and ethanol absolute (≥99.7%, CH_3CH_2OH) were purchased from Sinopharm Chemical Co., Ltd (Shanghai, China). Magnesium sulphate (≥99.0%, $MgSO_4\cdot 7H_2O$), cupric nitrate (99.5%, $Cu(NO_3)_2\cdot 3H_2O$) and urea (≥99.0%, H_2NCONH_2) were purchased from Guangcheng Chemical Co., Ltd (Tianjin, China). Sodium hydroxide (≥96%, NaOH) and hydrochloric acid (36%–38%, HCl) were purchased from Dengke Chemical Co., Ltd (Tianjin, China). Congo red ($C_{32}H_{22}N_6Na_2O_6S_2$) was purchased from Tianjin Chemical Co., Ltd (China). Kapok template was natural kapok cotton obtained from the local market, which was imported from Indonesia.

2.2. Synthesis of the γ-AlO(OH)/CuMgAl-LDH

In this study, kapok was used as the biological template. At first, the kapok was took into the boiling water for 5 min and dried for the next step. 0.4 g treated kapok was dipped into ethanol (C_2H_5OH) solution containing $Al(NO_3)_3\cdot 9H_2O$ (0.25 mol) and then ultrasound for 1 h. After dried at 80°C for 12 h, the samples were calcined at 550°C for 1 h, obtaining hollow fibers of Al_2O_3.

According to a certain molar ratio, $Al(NO_3)_3\cdot 9H_2O$, $MgSO_4\cdot 7H_2O$, 0.16 g of urea, and $Cu(NO_3)_2\cdot 3H_2O$ were dissolved in 30 mL distilled water and 0.16 g of the pretreated kapok was dipped in the mixed solution. Then the mixed solution was transferred to Teflon-lined stainless autoclave and further treated for 15 h at 80°C, 120°C and 160°C, respectively. The product was collected by filtration and repeatedly washed with deionized water. Finally, the as-prepared sample were dried at 80°C. Depending on the special hydrothermal temperature, the obtained samples were designated γ-AlO(OH)/CuMgAl-LDH-N, where N was the hydrothermal temperature.

2.3 Adsorption experiments

Congo Red (CR) was used to test the adsorption perpormance of the as-prepared samples. 50 mg γ-AlO(OH)/CuMgAl-LDH was added into 100 mL CR solutions with the initial concentration of 50 mg L^{-1}. 5 mL of the solution was analyzed after various time intervals (1/6, 1/2, 1, 2, 3, 5, 10, 24 and 48 h) and centrifuged to remove the adsorbent.

The concentrations of CR before and after treatment were measured via UV-Visible spectrophotometer (U-3501, Hitachi, Japan). The adsorption capacity, q_e (mg g^{-1}), was obtained using the equation given by [21]:

$$q_e = \frac{(C_0 - C_e)\times V}{W} \quad (2)$$

where C_0 (mg/L) and C_e (mg/L) are the initial and equilibrium concentration of dyes, V (L) is the volume of dye solution and W (mg) is the weight of the synthesized adsorbent.

2.4. Characterizations

The structure and the crystalline phases of the as-prepared samples were investigated by X-Ray powder diffraction (XRD) with Cu Ka radiation (λ = 0.1540 nm). The samples were operated at 40 KV and 100 mA and the measurements were done at 2θ values ranging from 5° to 80°. The morphology and the elements composition of the samples were analyzed by field emission-scanning electron microscopy (SEM) and high resolution transmission electron microscopy (HRTEM, Tecnai F20, Philips, Hillsboro, OR, USA) equipped with EDS. FT-IR spectra of the samples were recorded on FT-IR spectrometer (Thomas Nicolet 380, USA) with the spectral range of 4000–500 cm^{-1}. The pore structures of the as-prepared samples were measured by nitrogen adsorption-desorption at 77 K with a surface area analyzer (ASAP2020M+C, Micrometrics). The elemental composition on the surface of as-prepared samples was characterized by X-ray photo-electron spectra (XPS) analysis on a VG ESCALAB MKII XPS system with Al K X-ray as the excitation. The surface areas of samples were estimated by the Langmuir model and Brunauer–Emmett–Teller (BET) model. The Barrett Joyner Halenda (BJH) theory was used to estimate the pore size distribution of the samples. Thermogravimetric Ananlysis (TG), obtained by a thermal analyzer (NETZSCH STA 449), was used to analyze the thermal stability of the product.

3. Result and discussion

3.1. Structural characterization

The XRD patterns of kapok template and γ-AlO(OH)/CuMgAl-LDH obtained at different hydrothermal temperatures (80°C, 120°C and 160°C) are shown in Fig. 1a. For the pre-treated kapok, one broad peak could be observed clearly, which should be attributed to the amorphous Al_2O_3 phase. For the γ-AlO(OH)/CuMgAl-LDH samples hydrothermally treated at 80°C, no significant diffraction peak appeared. With the increasing hydrothermal temperature, the diffraction peaks of γ-AlO(OH) and CuMgAl-LDH became shaper and the intensities indicated the grain growths of γ-AlO(OH) and CuMgAl-LDH. The significant characteristic peaks of CuMgAl-LDH were located at 11.2°, 22.7°, 33.4° and 35.6°, responding to the (003), (006), (012) and (009) of CuMgAl-LDH, while the characteristic peaks of the γ-AlO(OH) were observed at 13.8° and 27.8°, corresponding to the (020) and (120) of γ-AlO(OH). Moreover, the peaks that appeared at 16.5° and 23.4° indicated the presence of $Mg_2CO_3(OH)_2{\cdot}3H_2O$ impurity phase. This may be due to excess content of Mg^{2+},which could react with OH^- and CO_3^{2-} to form the phase of $Mg_2CO_3(OH)_2{\cdot}3H_2O$. However, hydroxyl derived from $Mg_2CO_3(OH)_2{\cdot}3H_2O$ could also make some contributions to the adsorption of dye. Potential impurities could be removed by dilute acid.

FTIR spectroscopy of the as-synthesized γ-AlO(OH)/CuMgAl-LDH-160 is shown in Fig. 1b. As is shown, most of the FTIR bands in the spectrum could be appointed established in the contrast with those of γ-AlO(OH) and CuMgAl-LDH. The peaks at 1358 and 669 cm^{-1} may be ascribed to stretching absorption of CO_3^{2-} in C–O from the LDH. The bands at 859, 720 and 583 cm^{-1} could be assigned to the Al/Mg/Cu-O vibration absorption from CuMgAl-LDH. The band at 3462 cm^{-1} obviously may be correlated to the stretching vibration of –OH. The bands at 1072, 1382, 1636 cm^{-1} could be ascribed to the stretching and bending vibration absorption in Al-OH.

The TG curve of γ-AlO(OH)/CuMgAl-LDH-160 is shown in Fig. 1c. It could be observed that the weight of γ-AlO(OH)/CuMgAl-LDH-160 decreased with the increase of the temperature and then tended to a stable value. There are three stages of weightlessness in γ-AlO(OH)/CuMgAl-LDH-160 during the thermal decomposition process. When the temperature was below 280°C, the weightlessness could be associated with the removal of crystal water. Between 250°C to 450°C, it could be corresponded to the decomposition of interlayer carbonate and hydroxyl. Mixed

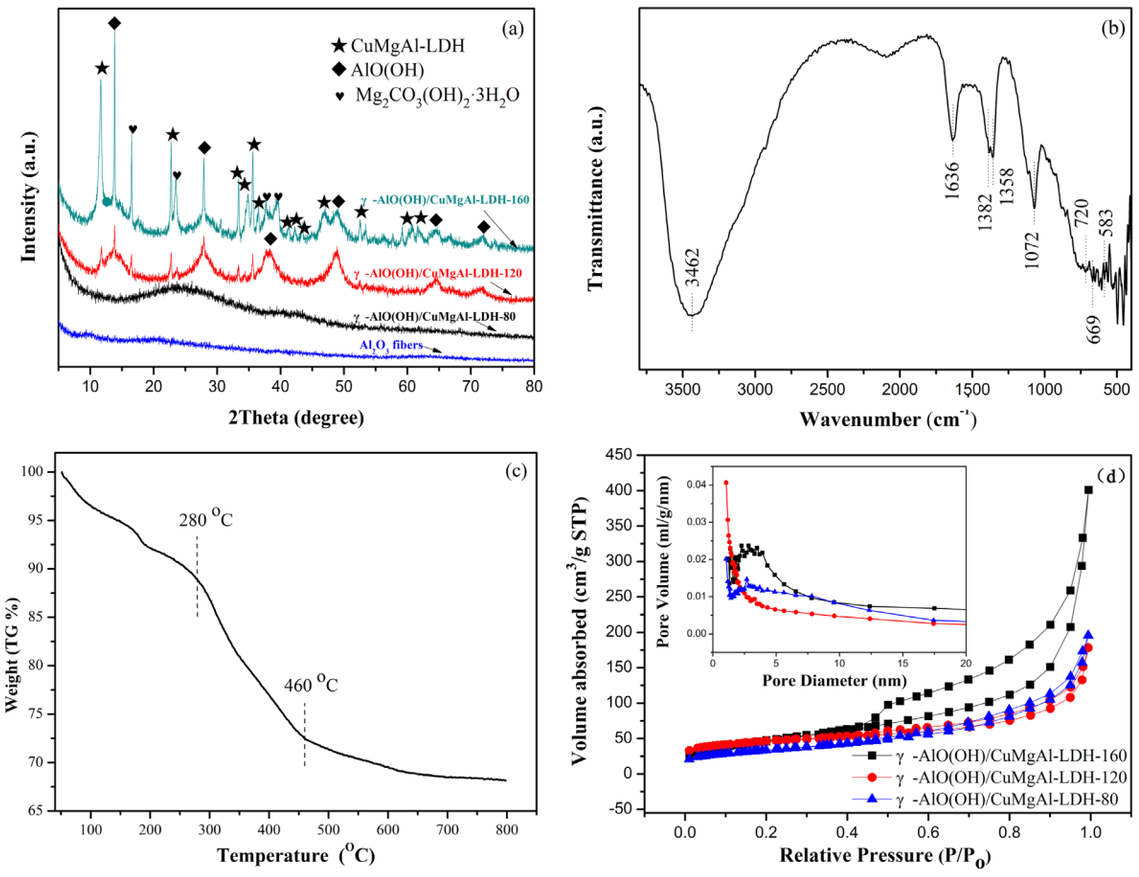

Fig. 1. XRD patterns of Al_2O_3 fibers, γ-AlO(OH)/CuMgAl-LDH-80, γ-AlO(OH)/CuMgAl-LDH-120 and γ-AlO(OH)/CuMgAl-LDH-160 (a), IR spectra(b), and TG curve(c), and N_2 adsorption-desorption isotherm and BJH pore size distribution(inset) (d) of γ-AlO(OH)/CuMgAl-LDH-80, γ-AlO(OH)/CuMgAl-LDH -120 and γ-AlO(OH)/CuMgAl-LDH-160.

metal oxides were obtained when the calcination temperature was above 460°C [22].

The adsorption capacity of the material could be influenced by the pore structure and specific surface area, since more active binding sites are available on a material with higher surface area. The nitrogen adsorption–desorption isotherms and pore size distribution of the as-obtained samples are shown in Fig. 1d. According to the classification of the IUPAC[23], N_2 adsorption isotherm of γ-AlO(OH)/CuMgAl-LDH-80, γ-AlO(OH)/CuMgAl-LDH-120 and γ-AlO(OH)/CuMgAl-LDH-160 belonged to type IV adsorption isotherm, which had hysteresis loop due to the capillary condensation. When the P/P_o increased, it showed the phenomenon of capillary condensation firstly and achieved the adsorption saturation later, which implied that prepared γ-AlO(OH)/CuMgAl-LDH-160 belonged to the mesoporous material (2–50 nm). The specific surface area and the total pore volumes, calculated by the BET model [24] were 137.161, 144.537 and 167.638 $m^2 g^{-1}$ for γ-AlO(OH)/CuMgAl-LDH-80, γ-AlO(OH)/CuMgAl-LDH-120 and γ-AlO(OH)/CuMgAl-LDH-160, respectively. The corresponding pore volumes were 0.257, 0.303 and 0.633 $cm^3 g^{-1}$.

XP spectra (Fig. 2) were used to determine the chemical composition and elemental chemical status of the prepared samples. It can be found that the γ-AlO(OH)/CuMgAl-LDH-160 is composed of Cu 2p, Mg 1s, C 1s, O 1s and Al 2p peaks in Fig. 2a. As shown in Fig. 2b, the peaks at binding energy of 953.9, 933.6 eV could be attributed to Cu $2p_{1/2}$ and Cu $2p_{3/2}$, respectively. In addition, the shake-up satellite peaks at 963.1 and 937.9–945.4 eV confirmed the presence of Cu^{2+}. We could see that the peak in Mg 1s spectrum (Fig. 2c) at 1303.0 e V could be assigned to $Mg(OH)_2$ derived from the LDH structure. The characteristic Al 2p peaks (Fig. 2d) at 76.6 and 74.3 eV could be assigned to Al^{3+} derived from the LDH structure and γ-AlOOH, respectively. The XPS results are consistent with the above XRD and IR results to indicate the formation of γ-AlO(OH)/CuMgAl-LDH-160.

Further FESEM study was used to get more information about as-synthesized samples. Fig. 3a shows that kapok template had hollow fibrous structure with smooth surface and uniform diameter (about 15 μm). The SEM image of Al_2O_3 fiber is shown in Fig. 3b. Fig. 3c and Fig. 3d show the SEM images of γ-AlO(OH)/CuMgAl-LDH-160. As it was observed, the product retained the microstructure of kapok fibers, which could provide more space for the growth of the LDH nanosheets. Furthermore, it also provided limited growth region of the LDH sheets and was able to control the morphology as expected. The obtained CuMgAl-LDH were hexagonal nanosheets, which had the irregular edges but uniform size. γ-AlO(OH) had the honeycombed structure, providing more specific surface areas and pore structure to enhance its absorption capacity. The homologous EDS spectrum (Fig. 3e) shows a Cu: Mg: Al atomic ratio of around

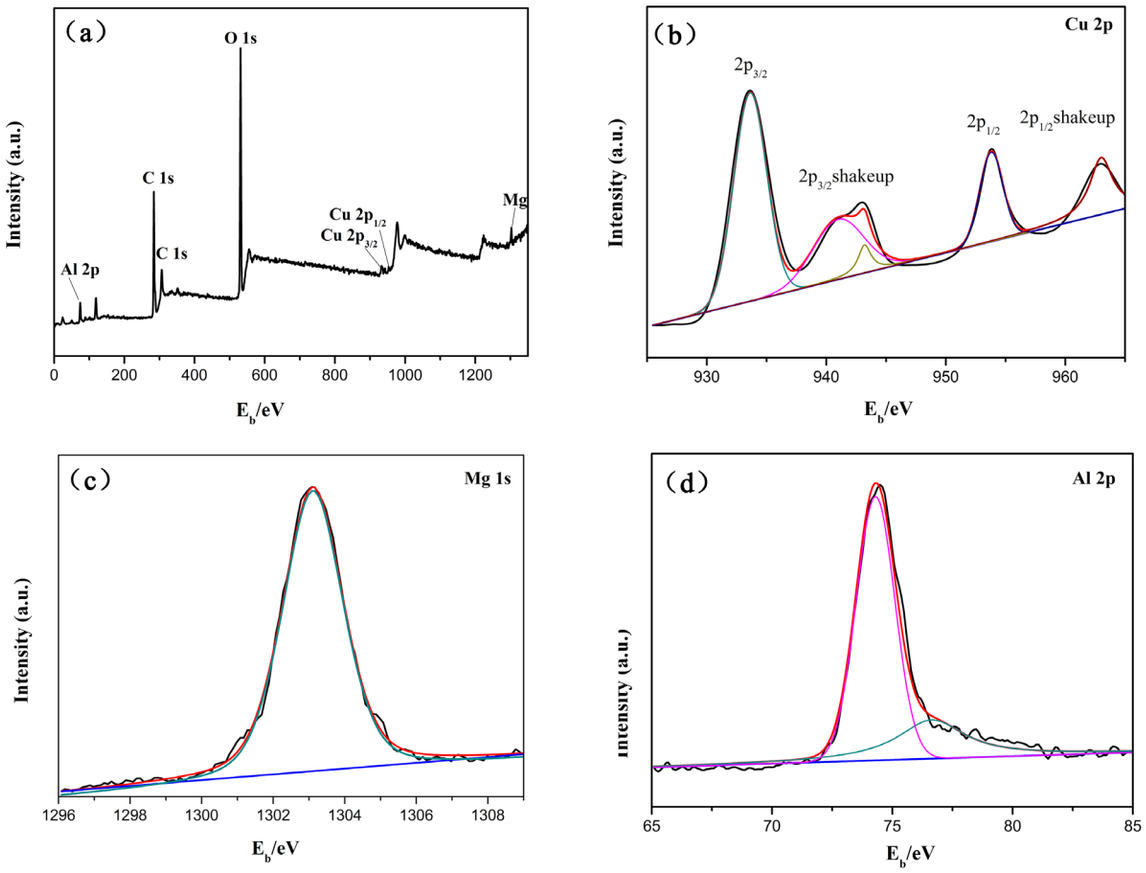

Fig. 2. XP spectra of γ-AlO(OH)/CuMgAl-LDH-160 (a) survey spectrum, (b) Cu 2p XP spectra, (c) Mg 1s,and (d) Al 2p XP spectra.

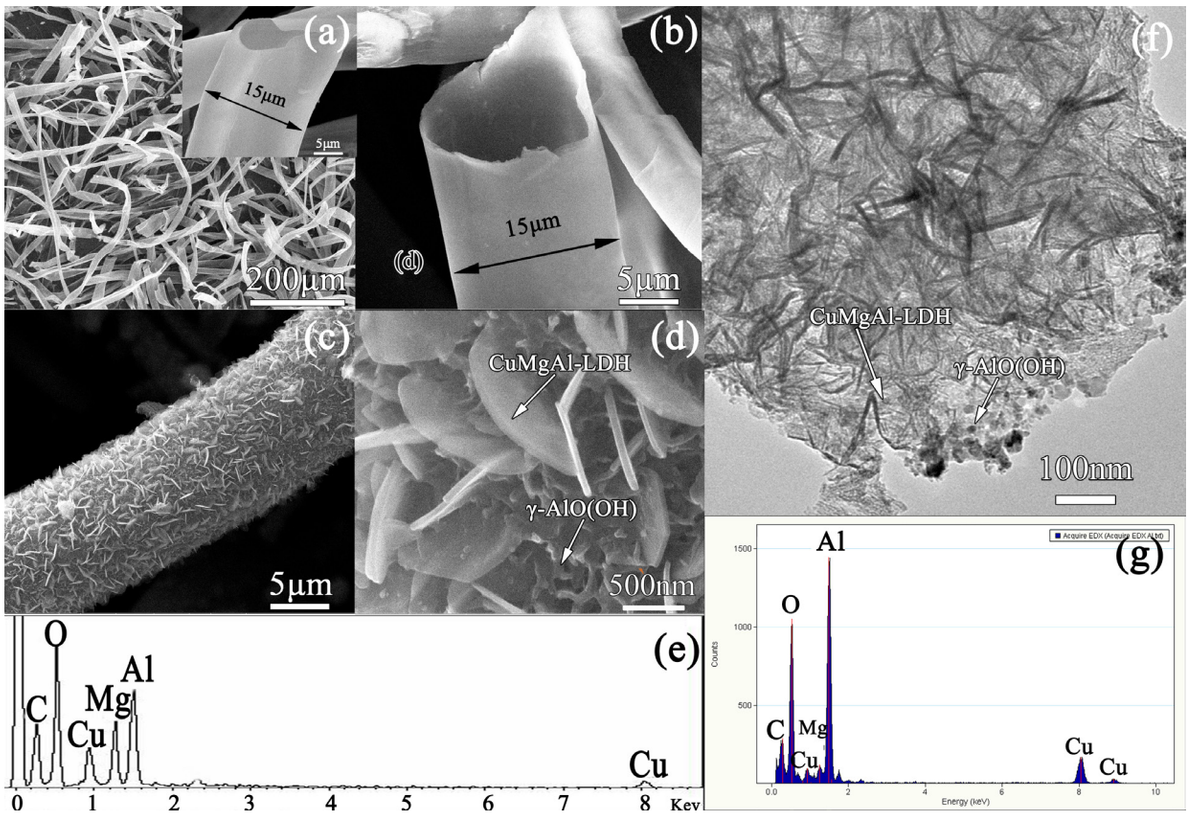

Fig. 3. SEM images of kapok (a), Al_2O_3 fibers (b), (c–d), homologous EDS spectrum of γ-AlO(OH)/CuMgAl-LDH-160; TEM. image (f) and homologous EDS spectrum (g) of γ-AlO(OH)/CuMgAl-LDH-160.

2.87:4.94:6.30. The spectra clearly demonstrate the presence of copper, magnesium, aluminum, oxygen, and carbon, which is in good agreement with the XRD observations. The structure and morphology of as-synthesized samples observed by TEM is shown in Fig. 3f and the homologous EDS spectrum is shown in Fig. 3g. The TEM image implied that CuMgAl-LDH revealed polygon sheet-like structure and the γ-AlOOH exhibited black dots in the TEM images, which was consistent with the results of SEM.

According to the above study, the possible mechanism of the synthesis of the samples was proposed. For Al_2O_3 fibers, firstly, precursor solution of AlO^+ was attracted by active groups (–OH, –COOH and $–OCH_3$) from cotton cellulose according electrostatic interactions. During the calcination, kapok fibers decomposed to produce CO_2 and H_2O gradually. Then the structures of the samples tended to be stable and the amorphous Al_2O_3 fibers were obtained ultimately, which retained the morphology of the kapok template. γ-AlO(OH)/CuMgAl-LDH was synthesized with urea hydrothermal method, which could effectively control the grain size of the crystal phase at high temperature and pressure. In this way, the interlayer anions dispersed better, which could contribute to the regular structure and morphology. Urea was used as the precipitant to provide alkaline environment, because it would be decomposed into ammonia and carbon dioxide above 80°C. The reaction equations are shown as:

$$3\,H_2O + (NH_2)CO \rightarrow 2\,NH_3{\cdot}H_2O + CO_2\uparrow \quad (3)$$

$$NH_4^+ + OH^- \leftrightarrow NH_3{\cdot}H_2O \leftrightarrow NH_3\uparrow + H_2O \quad (4)$$

Urea decomposed when heated to a certain temperature to produce OH^- and then attracted Cu^{2+}, Mg^{2+} and Al^{3+} to the surface of Al_2O_3 fibers, contributing to crystallization and nucleation of the γ-AlO(OH) and CuMgAl-LDH rapidly. Through the effect of hydrogen bonding, γ-AlO(OH) and CuMgAl-LDH grew in situ on the surface of fibers by following reactions:

$$Al^{3+} + 3\,OH^- \rightarrow Al(OH)_3 \rightarrow \gamma\text{-}AlO(OH) + H_2O$$
$$2\,OH^- + (x+y+1.5z-1)\,CO_3^{2-} + x\,Cu^{2+} + y\,Mg^{2+} + z\,Al^{3+} + n\,H_2O \quad (5)$$

$$Cu_xMg_yAl_y(OH)_2(CO_3)_{x+y+1.5z-1}{\cdot}nH_2O \quad (6)$$

3.2. Adsorption performance

Two kinetic models, pseudo-first-order and pseudo-second-order, were introduced to explore the adsorption kinetics of γ-AlO(OH)/CuMgAl-LDH. The pseudo-first-order was given as [25]:

$$\ln(q_e - q_t) = \ln q_e - K_1 t \quad (7)$$

where q_e and q_t are the adsorption capacity (mg g^{-1}) at equilibrium and at time t (h), respectively. K_1 is the adsorption rate constant of pseudo-first-order. The pseudo-second-order was given as [26]:

$$\frac{t}{q_t} = \frac{1}{K_2 q_e^2} + \frac{t}{q_e} \tag{8}$$

where q_e (mg g^{-1}) is the adsorption capacity at equilibrium and q_t is the adsorption capacity at any time t (h). K_2 is the adsorption rate constant of pseudo-second-order.

The fitting diagrams of dynamics simulation from γ-AlO(OH)/CuMgAl-LDH-80, γ-AlO(OH)/CuMgAl-LDH-120 and γ-AlO(OH)/CuMgAl-LDH-160 are shown in Fig. 4a–b. The fitting parameters of pseudo-first-order and pseudo-second-order are shown in Table 1. It was important to note that the R^2 in the pseudo-second-order was higher than in the pseudo-first-order, which meant the pseudo-second-order was fit to characterize the program of adsorption. For CR, γ-AlO(OH)/CuMgAl-LDH-160 had the maximum saturated adsorption capacity of 155.76 mg g^{-1}. The relationship between the contact time and adsorption capacity of γ-AlO(OH)/CuMgAl-LDH-80, γ-AlO(OH)/CuMgAl-LDH-120 and γ-AlO(OH)/CuMgAl-LDH-160 is shown in Fig. 4c. At the early time, the adsorption of CR increased significantly, then slowed down and tended to saturation after 48 h. γ-AlO(OH)/CuMgAl-LDH-160 showed the best performance in the adsorption of CR and the color of CR changed from red to transparent, which was corresponding to the adsorption process. The sharp increase of adsorption amount in the early stages should attribute to the large content of unsaturated adsorption sites. Organic functional groups of CR could be adsorbed on γ-AlO(OH)/CuMgAl-LDH-160 by electrostatic interactions. After a long time, a slow adsorption process appeared because of the reduced adsorption sites. It can be seen from Fig. 4d that the adsorption capacity of template-free γ-AlO(OH)/CuMgAl-LDH-160 was much weaker than that of the sample synthesized by the biological template method. The reason may be that the application of the bio-template method allows the prepared material having porous 3D structure. This 3D porous

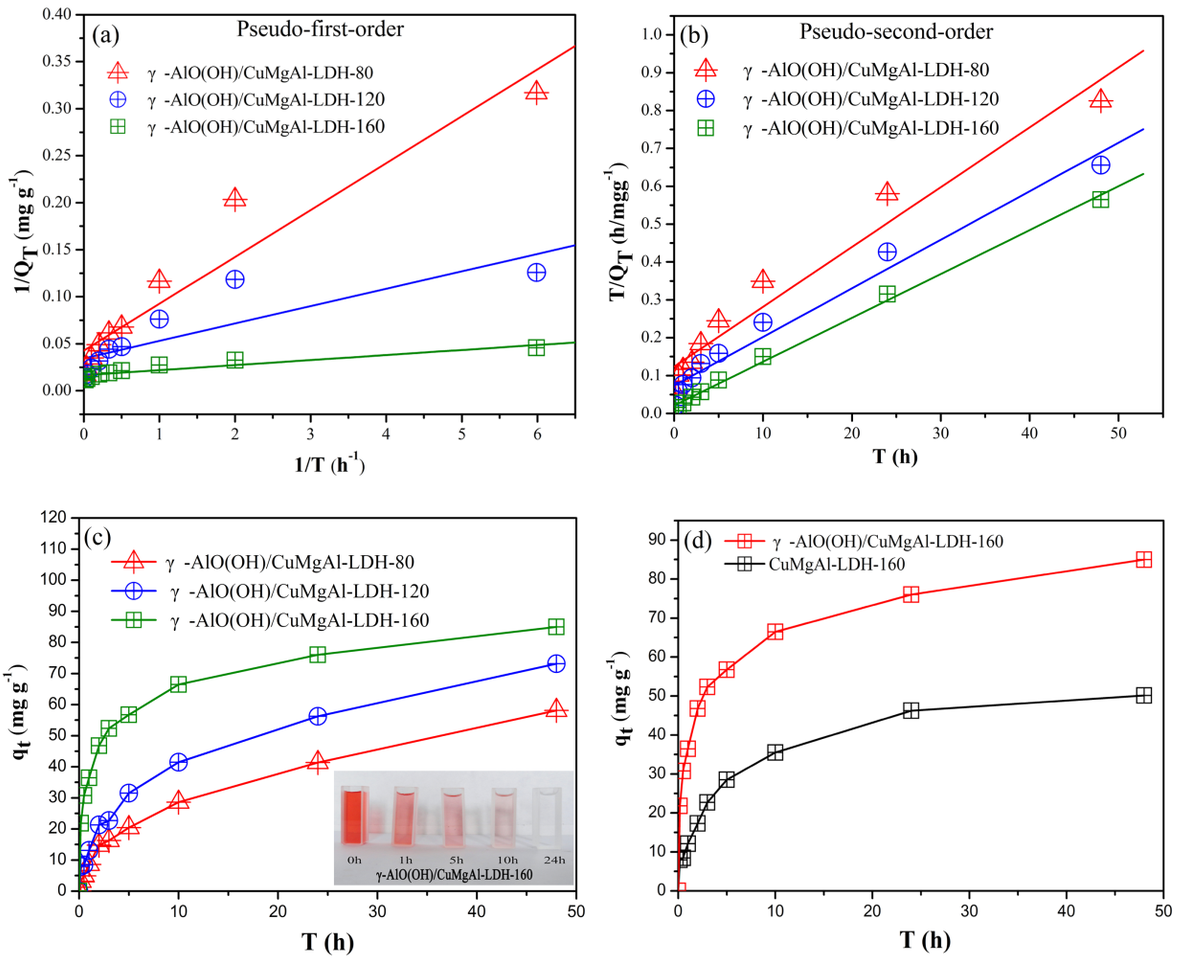

Fig. 4. Linear fitting of pseudo-first-order (a), and pseudo-second-order (b), effect of contact time on adsorption capacity (c) of γ-AlO(OH)/CuMgAl-LDH-80, γ-AlO(OH)/CuMgAl-LDH-120 and γ-AlO(OH)/CuMgAl-LDH-160 and effect of template on adsorption performance of γ-AlO(OH)/CuMgAl-LDH-160 (PH = 6).

Table 1
Parameter of kinetic model

Kinetic model	Parameter	γ-AlO(OH)/ CuMgAl-LDH-80	γ-AlO(OH)/ CuMgAl-LDH-120	γ-AlO(OH)/ CuMgAl-LDH-160
Pseudo first-order	q_e (mg/g)	49.83	72.62	69.54
	K_1 (h^{-1})	4.68	0.30	0.41
	R^2	0.9423	0.6697	0.7538
Pseudo second-order	q_e (mg/g)	62.27	81.23	85.62
	K_2 (g/mgh)	0.01	0.01	0.01
	R^2	0.9779	0.9958	0.9951

structure combined with the lamellar LDH form a 3D open structure, which could increase the transport speed of solution, provide more active sites, and improve the adsorption performance.

Langmuir and Freundlich models were introduced to learn the adsorption isotherms. The Langmuir isotherm is given by:

$$\frac{C_e}{q_e} = \frac{1}{q_{\max} K_L} + \frac{C_e}{q_{\max}} \tag{9}$$

$$R_L = \frac{1}{1 + K_L C_0} \tag{10}$$

where C_0 (mg L^{-1}) and C_e (mg L^{-1}) are the initial and equilibrium concentration of dyes and q_e (mg g^{-1}) is the amount of the dye adsorbed at equilibrium. K_L (L mg^{-1}) is the Langmuir adsorption constant, corresponding to the strength of adsorption capacity [26], and q_{max} is the maximum saturated adsorption amount of surface monolayer onto the adsorbent. The Freundlich isotherm is given as:

$$\lg q_e = \lg K_F + \frac{1}{n} \lg C_e \tag{11}$$

where K_F (L mg^{-1}) is Freundlich adsorption constant and n is empirical parameters. Langmuir and Freundlich isotherm models of γ-AlO(OH)/CuMgAl-LDH-160 are shown in Fig. 5a–b and the relationship between the initial concentration and adsorption capacity is exhibited in Fig. 5c. Accordingly, the parameters of isotherm models are shown in Table 2. It could be observed that R^2 in Langmuir model was significantly higher than that in Freundlich model, which means the adsorption of CR onto γ-AlO(OH)/CuMgAl-LDH-160 was monolayer. Accordingly, γ-AlO(OH)/CuMgAl-LDH-160 had the maximum monolayer adsorption capacity of 155.76 mg g^{-1}. Absorbents of various materials for CR are shown in able Table 3. It could be seen that as-synthesized sample makes a good performance in adsorption of CR. In addition, dispersion coefficient R_L was related to the shape of the isotherm, which was judging whether the adsorption reaction was unfavorable (R_L > 1), favorable (0< R_L <1), linear (R_L = 1) or irreversible (R_L = 0). In this work, R_L calculated from the equation was 0.02, indicating that the adsorption of CR was favorable. It also could be proved in Freundlich isotherm model. Index magnitude $1/n$ gives an indication of the favorable adsorption. When n > 1 (n = 19.19), it represents a favorable adsorption conditions.

The pH value is a significant parameter in adsorption process, which can influence the adsorption amount of as-synthesized samples toward CR. Fig. 5d shows the effect of pH values on the adsorption of the CR onto γ-AlO(OH)/CuMgAl-LDH-160. The pH was studied from 3 to 11. The adsorption of CR decreased with the increasing pH value, indicating that the adsorbent made better performance in the adsorption of CR in acidic or neutral reaction conditions. Molecular anionic dye (D-SO_3^-) and cations (Na^+) could be generated by the ionization of D-SO_3 Na of the aqueous solution CR:

$$\mathrm{D-SO_3Na} \xrightarrow{\mathrm{H_2O}} \mathrm{D-SO_3^-} + \mathrm{Na^+} \tag{12}$$

As some published literatures reported, the pH_{pzc} of LDHs was larger than 9.5 [42]. When the pH < PH_{pzc}, the LDH was positively charged. In that situation, it facilitated the electrostatic attraction of SO_3^- of CR onto the adsorbent. Otherwise, in the higher pH range, the SO_3^- would be repelled by the LDH. While the density of laminates positive charge increased in acid environment, the repulsion between the laminates enhanced, facilitating the introduction of adsorbate into the interlayer.

For adsorbent, the temperature of the adsorption system is an important factor. The influence of reaction temperature on the adsorption capacity is shown in Fig. 6a. It can be observed that the adsorption capacity increased with increasing temperature within a certain range. To further investigate the thermodynamics from the adsorption of CR, three parameters (standard enthalpy change (ΔH°), the standard free energy change (ΔS°) and the standard Gibbs energy change (ΔG°)) were obtained from the equations given by:

$$\ln Ka = \frac{\Delta S^o}{R} - \frac{\Delta H^o}{RT} \tag{13}$$

$$\mathrm{K}\alpha = \frac{q_e}{C_e} \tag{14}$$

$$\Delta G^o = -RT \ln Ka \tag{15}$$

where T (K) is the temperature of the solution and $K\alpha$ is the constant of equilibrium adsorption. R is the atmospheric constant 8.3144 J mol^{-1} K^{-1}.

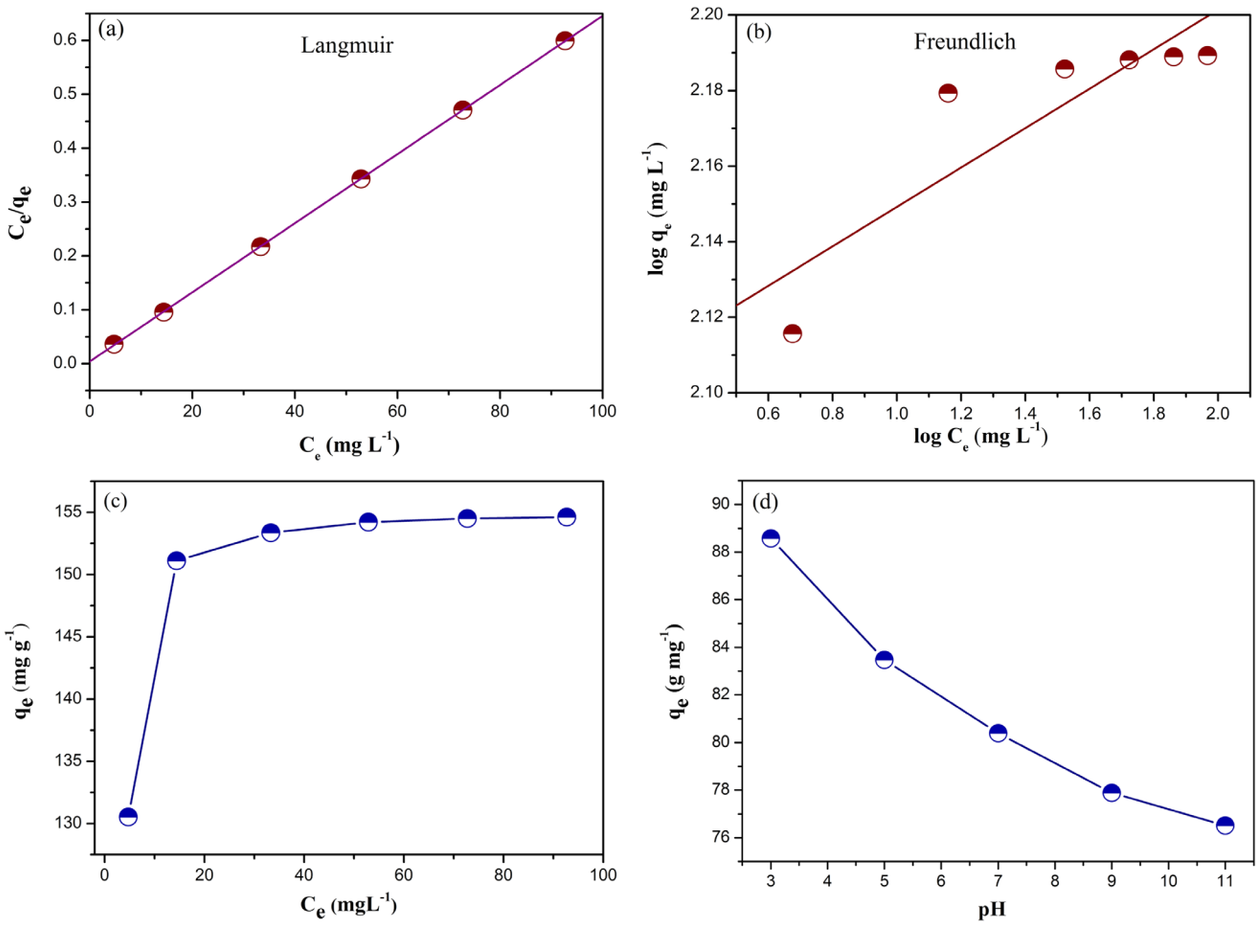

Fig. 5. Langmuir (a), and Freundlich (b) isotherm model, and effect of initial concentration (PH = 6) (c) and pH value (d) on the adsorption capacity (γ-AlO(OH)/CuMgAl-LDH-160, 0.05 g, 100 mL, 50 mg L^{-1}).

Table 2
Parameters of isotherm models

Isotherm models	Parameter	Value
Langmuir	K_L (L mg^{-1})	0.09
	q_{max} (mg g^{-1})	155.76
	R_L	0.02
	R^2	0.9997
Freundlich	K_F (L mg^{-1})	125.03
	n	19.19
	R^2	0.7123

$\Delta H°$ and $\Delta S°$ were calculated by the slope and intercept of the curve (Fig. 6b) and the results are summarized in Table 4. It could be seen that $\Delta H°$ (52.90 KJ mol^{-1}) was positive, proving that the adsorption reaction was endothermic. As for $\Delta G°$ with negative values, which indicated the reaction was spontaneous, reduced from –2.38 KJ mol^{-1} (30°C) to –9.85 KJ mol^{-1} (70°C) and this could confirm the view that increasing temperature promoted the adsorption of CR. In addition, $\Delta S°$ (182.99 J mol^{-1} K^{-1}) was positive, indicating that the entropy in the system of adsorption-desorption was increased.

Further UV–visible spectra and FTIR were used to investigate the mechanism of adsorption of as-synthesized sample. Fig. 7a exhibits the variation of UV-Visible spectra of aqueous solutions of CR after various time intervals upon the addition of the γ-AlO(OH)/CuMgAl-LDH-160. With the increasing of the adsorption time, absorption spectra changed gradually. It could be pointed that the concentrate of CR obviously decreased in the first 5 h and then gradually slowed down. FTIR of CR, γ-AlO(OH)/CuMgAl-LDH-160 (before adsorption), γ-AlO(OH)/CuMgAl-LDH-160 (after adsorption) are shown in Fig. 7b, respectively. As it was shown, the peaks at 3462 cm^{-1}, 1636 cm^{-1} and 1358 cm^{-1} became weak, showing a decrease in the content of hydroxyl groups and CO_3^{2-} on the adsorbent, which indicated that hydroxy and CO_3^{2-} were involved in the process of adsorption. The band at 1176 cm^{-1} of γ-AlO(OH)/CuMgAl-LDH-160 after adsorption significantly had an additional peak, which was assigned to the symmetric and asymmetric absorption peak of sulfonic group (S=O) of CR. The fingerprint region (590 cm^{-1} ~1030 cm^{-1}) also had

Table 3
Adsorption capacity of CR onto various adsorbents

q_{max}(mg g^{-1})	Absorbent	References
155.76	γ-AlO(OH)/CuMgAl-LDH-160	This work
107.41	Ca-bentonite	[27]
59.50	Porous ZrO_2 hollow sphere	[28]
141.64	La_2O_3-doped TiO_2 nanotubes	[29]
526.30	237 nm NiO	[30]
176.70	γ-Al_2O_3	[31]
35.84	Na bentonite(clay materials)	[32]
253.8	Iron oxide (α-Fe_2O_3) nanoparticles and nanowhiskers	[33]
113.6	Hollow microspheres $Ni(OH)_2$–Si	[34]
117.5	$Mg(OH)_2$–GO 0.5%	[35]
167.73	NiO nanosheets	[36]
241.5	Co Fe_2O_4(S5)	[37]
357	NiO–Al_2O_3	[38]
277.78	Leonardite(900)	[39]
163	CMOPP	[40]
123.89	Ni O/graphenenanosheets (NGNS)	[41]

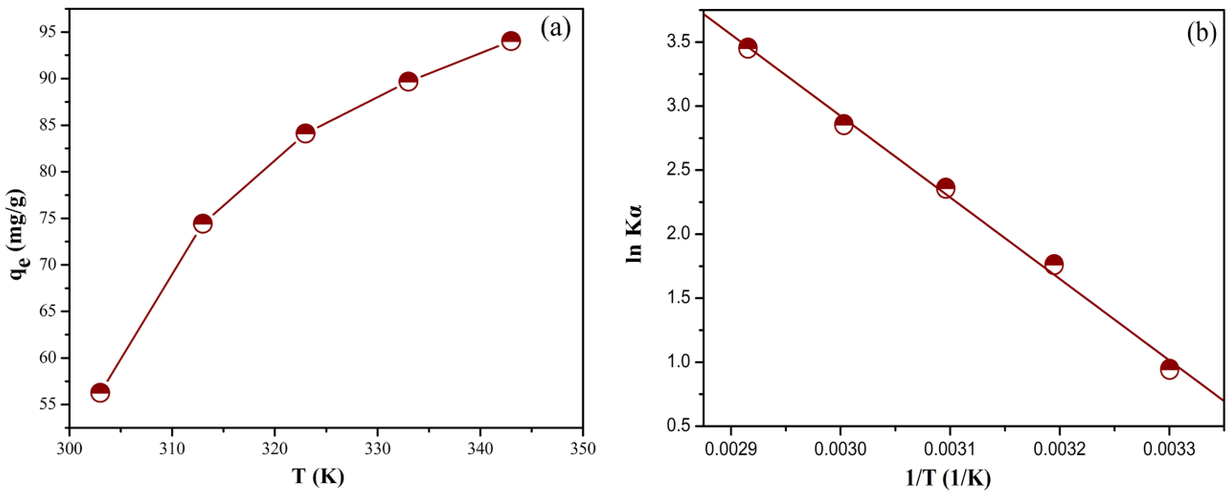

Fig. 6. Effect of temperature on the adsorption capacity (a), and Van's Hoff plot of adsorption of CR (b) (γ-AlO(OH)/CuMgAl-LDH-160, 0.05 g, 100 mL, 50 mg L^{-1} PH = 6).

Table 4
Thermodynamic parameters of adsorption of γ-AlO(OH)/CuMgAl-LDH-160

Concentration (mg/L)	ΔH° (KJ mol^{-1})	ΔS° (J mol^{-1} K^{-1})	ΔG° (KJ mol^{-1}) with different temperatures (°C)				
			30	40	50	60	70
100	52.90	182.99	–2.38	–4.58	–6.33	–7.90	–9.85

a significant change because of impact of the introduced new groups of CR, proving the adsorption of CR onto γ-AlO(OH)/CuMgAl-LDH-160. According to the analysis of FTIR, adsorption thermodynamics, adsorption isotherm model, effects of PH and UV–visible spectra of γ-AlO(OH)/CuMgAl-LDH-160, the mechanism of adsorption toward CR included electrostatic attraction of surface charge, hydrogen bond and anion exchange interlayer.

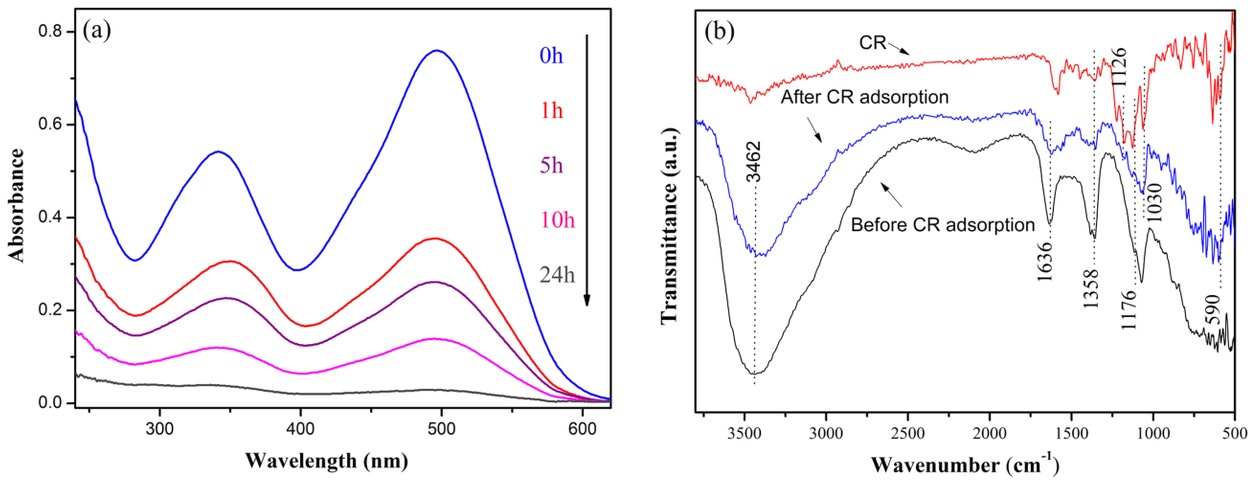

Fig. 7. UV-visible absorption spectra during adsorption process of CR (a), FTIR spectra of CR, γ-AlO(OH)/CuMgAl-LDH-160, and γ-AlO(OH)/CuMgAl-LDH-160 adsorbed with CR(b) (γ-AlO(OH)/CuMgAl-LDH-160, 0.05 g, 50 mg L^{-1}, 100 mL).

4. Conclusion

In summary, biomorphic hierarchical γ-AlO(OH)/CuMgAl-LDH was synthesized by combining the bio-templated and hydrothermal method. 2D LDH nanosheets and honeycomb γ-AlO(OH) were fabricated into 3D biomorphic micro-nano structures by means of in situ growth, which exhibited high adsorption capacity toward CR. The maximum saturated adsorption capacity toward CR was 155.76 mg g^{-1}. It was found that the CR adsorption process could be well matched with the pseudo-second-order model and Langmuir model, respectively. According to the thermodynamic analysis, the CR adsorption onto γ-AlO(OH)/CuMgAl-LDH was spontaneous and endothermic. The main adsorption mechanisms of γ-AlO(OH)/CuMgAl-LDH included electrostatic adsorption of surface charges, hydrogen bond and anion exchange interlayer.

Acknowledgement

This work was supported by the National Natural Science Foundation of China (Grant No. 51672110), National Natural Science Foundation of China (Grant No.51401085), Natural Science Foundation of Shandong Province (No. 2015ZRB019N1), the HKSAR Government RGC-GRF Grant (CUHK14303914) and the Direct Grant (Project Code: 4053076) from the Faculty of Science of the Chinese University of Hong Kong.

References

[1] Z. Wang, N. Bramnik, S. Roy, G.D. Benedetto, J.L.Z. Iii, S. Mitra, Flexible zinc–carbon batteries with multiwalled carbon nanotube/conductive polymer cathode matrix, J. Power Sources, 237 (2013) 210–214.

[2] K. Feng, D. Rong, W. Ren, X. Wen, Hierarchical flower-like γ-AlOOH and γ-Al_2O_3 microspheres: Synthesis and adsorption properties, Mater. Express, 5 (2015) 371–375.

[3] H. Hou, Y. Zhu, G. Tang, Q. Hu, Lamellar γ-AlOOH architectures: Synthesis and application for the removal of HCN, Mater. Charact., 68 (2012) 33–41.

[4] H. Huang, L. Wang, Y. Cai, C. Zhou, Y. Yuan, X. Zhang, H. Wan, G. Guan, Facile fabrication of urchin-like hollow boehmite and alumina microspheres with a hierarchical structure via Triton X-100 assisted hydrothermal synthesis, Cryst. Eng. Comm., 17 (2015) 1318–1325.

[5] W.Q. Jiao, X.M. Liang, Y.M. Wang, M.-Y. He, Formation of hierarchical boehmite with different nanostructures in dry-gel conversion process, Cryst. Eng. Comm., 16 (2014) 3348–3358.

[6] J.F. Bringley, T.A. Qiao, Silylamine modified nanoparticulate carriers, in, US, 2005.

[7] X. Yu, J. Yu, B. Cheng, M. Jaroniec, Synthesis of hierarchical flower-like AlOOH and TiO_2/AlOOH Superstructures and their enhanced photocatalytic properties, J. Phys. Chem. C, 113 (2009) 17527–17535.

[8] W. Cai, S. Chen, J. Yu, Y. Hu, C. Dang, S. Ma, Template-free solvothermal synthesis of hierarchical boehmite hollow microspheres with strong affinity toward organic pollutants in water, Mater. Chem. Phys., 138 (2013) 167–173.

[9] H. Huang, L. Wang, Y. Cai, C. Zhou, Y. Yuan, X. Zhang, H. Wan, G. Guan, Facile fabrication of urchin-like hollow boehmite and alumina microspheres with a hierarchical structure via Triton X-100 assisted hydrothermal synthesis, Cryst. Eng. Comm., 17 (2014) 1318–1325.

[10] J. Zhang, S. Wei, J. Lin, J. Luo, S. Liu, H. Song, E. Elawad, X. Ding, J. Gao, S. Qi, Template-free preparation of bunches of aligned boehmite nanowires, J. Phys. Chem. B, 110 (2006) 21680–21683.

[11] J. Zhou, S. Yang, J. Yu, Z. Shu, Novel hollow microspheres of hierarchical zinc–aluminum layered double hydroxides and their enhanced adsorption capacity for phosphate in water, J. Hazard. Mater., 192 (2011) 1114–1121.

[12] R. Selvakumar, N. Seethalakshmi, P. Thavamani, R. Naidu, M. Megharaj, Recent advances in the synthesis of inorganic nano/microstructures using microbial biotemplates and their applications, RSC Adv., 4 (2014) 52156–52169.

[13] X. Tian, W. He, J. Cui, X. Zhang, W. Zhou, S. Yan, X. Sun, X. Han, S. Han, Y. Yue, Mesoporous zirconium phosphate from yeast biotemplate, J. Colloid Interf. Sci., 343 (2010) 344–349.

[14] M. Huang, T. Li, N. Zhao, Y. Yao, H. Yang, C. Du, Y. Wang, Doping strontium in tricalcium phosphate microspheres using yeast-based biotemplate, Mater. Chem. Phys., 147 (2014) 540–544.

[15] Y. Xia, W. Zhang, Z. Xiao, H. Huang, H. Zeng, X. Chen, F. Chen, Y. Gan, X. Tao, Biotemplated fabrication of hierarchically porous NiO/C composite from lotus pollen grains for lithium-ion batteries, J. Mater. Chem., 22 (2012) 9209–9215.
[16] L. Yue, J. Guo, Q. Yang, X. Luo, J. Lian, J. Yang, L. Wang, Biotemplate synthesis of mesoporous iron phosphomolybdate supported on silica with enhanced photocatalytic property, Mater. Lett., 157 (2015) 225–227.
[17] J. Li, N. Zhang, D.H.L. Ng, Synthesis of a 3D hierarchical structure of γ-AlO(OH)/Mg–Al-LDH/C and its performance in organic dyes and antibiotics adsorption, J. Mater. Chem. A, 3 (2015) 21106–21115.
[18] T. Prakash, R. Jayaprakash, D.S. Raj, S. Kumar, N. Donato, D. Spadaro, G. Neri, Sensing properties of ZnO nanoparticles synthesized by using albumen as a biotemplate for acetic acid monitoring in aqueous mixture, Sensor Actuat. B. Chem., 176 (2013) 560–568.
[19] S.J. Bao, C. Lei, M.W. Xu, C.J. Cai, C.J. Cheng, C.M. Li, Environmentally-friendly biomimicking synthesis of TiO_2 nanomaterials using saccharides to tailor morphology, crystal phase and photocatalytic activity, Crystengcomm, 15 (2013) 4694–4699.
[20] C. Yin, S. Zhu, Z. Chen, W. Zhang, J. Gu, D. Zhang, One step fabrication of C-doped $BiVO_4$ with hierarchical structures for a high-performance photocatalyst under visible light irradiation, J. Mater. Chem. A, 1 (2013) 8367–8378.
[21] J. Zhou, C. Tang, B. Cheng, J. Yu, M. Jaroniec, Rattle-type carbon-alumina core-shell spheres: synthesis and application for adsorption of organic dyes, ACS Appl. Mater. Interfaces, 4 (2012) 2174–2179.
[22] E. Kanezaki, Thermal behavior of the hydrotalcite-like layered structure of Mg and Al-layered double hydroxides with interlayer carbonate by means of in situ powder HTXRD and DTA/TG, Solid State Ionics, 106 (1998) 279–284.
[23] K.S.W. Sing, Reporting physisorption data for gas/solid systems with special reference to the determination of surface area and porosity (Recommendations 1984), Pure Appl. Chem., 57 (1985) 603–619.
[24] P.D.L. Mercera, J.G.V. Ommen, E.B.M. Doesburg, A.J. Burggraaf, J.R.H. Ross, Influence of ethanol washing of the hydrous precursor on the textural and structural properties of zirconia, J. Mater. Sci., 27 (1992) 4890–4898.
[25] S. Lagergren, B.K. Svenska, About the theory of so-called adsorption of soluble substances, Handlingar, 24 (1898) 1–39.
[26] Y. Tan, J. Gu, X. Zang, W. Xu, K. Shi, L. Xu, D. Zhang, Versatile fabrication of intact three-dimensional metallic butterfly wing scales with hierarchical sub-micrometer structures, Angew. Chem. Int. Edit., 50 (2011) 8307–8311.
[27] L. Lian, L. Guo, C. Guo, Adsorption of Congo red from aqueous solutions onto Ca-bentonite, J. Hazard. Mater., 161 (2009) 126–131.
[28] C. Wang, Y. Le, B. Cheng, Fabrication of porous ZrO_2 hollow sphere and its adsorption performance to Congo red in water, Ceram. Int., 40 (2014) 10847–10856.
[29] H. Guo, J. Chen, W. Weng, Z. Zheng, D. Wang, Adsorption behavior of Congo red from aqueous solution on La_2O_3-doped TiO_2 nanotubes, J. Ind. Eng. Chem., 20 (2014) 3081–3088.
[30] B. Cheng, Y. Le, W. Cai, J. Yu, Synthesis of hierarchical Ni (OH) 2 and NiO nanosheets and their adsorption kinetics and isotherms to Congo red in water, J. Hazard. Mater., 185 (2011) 889–897.
[31] W. Cai, J. Yu, M. Jaroniec, Template-free synthesis of hierarchical spindle-like γ-Al_2O_3 materials and their adsorption affinity towards organic and inorganic pollutants in water, J. Mater. Chem., 20 (2010) 4587–4594.
[32] F.A. Pavan, S.L. Dias, E.C. Lima, E.V. Benvenutti, Removal of Congo red from aqueous solution by anilinepropylsilica xerogel, Dyes Pigments, 76 (2008) 64–69.
[33] T. Hao, C. Yang, X. Rao, J. Wang, C. Niu, X. Su, Facile additive-free synthesis of iron oxide nanoparticles for efficient adsorptive removal of Congo red and Cr(VI), Appl. Surf. Sci., 292 (2014) 174–180.
[34] C. Lei, X. Zhu, B. Zhu, J. Yu, W. Ho, Hierarchical NiO–SiO_2 composite hollow microspheres with enhanced adsorption affinity towards Congo red in water, J. Colloid Interf. Sci., 466 (2016) 238–246.
[35] M. Liu, J. Xu, B. Cheng, W. Ho, J. Yu, Synthesis and adsorption performance of $Mg(OH)_2$ hexagonal nanosheet–graphene oxide composites, Appl. Surf. Sci., 332 (2015) 121–129.
[36] J. Zhao, Y. Tan, K. Su, J. Zhao, C. Yang, L. Sang, H. Lu, J. Chen, A facile homogeneous precipitation synthesis of NiO nanosheets and their applications in water treatment, Appl. Surf. Sci., 337 (2015) 111–117.
[37] X. Wu, W. Wang, F. Li, S. Khaimanov, N. Tsidaeva, M. Lahoubi, PEG-assisted hydrothermal synthesis of $CoFe_2O_4$ nanoparticles with enhanced selective adsorption properties for different dyes, Appl. Surf. Sci., 389 (2016) 1003–1011.
[38] C. Lei, X. Zhu, Y. Le, B. Zhu, J. Yu, W. Ho, Hierarchically porous NiO-Al_2O_3 nanocomposite with enhanced Congo red adsorption in water, RSC Adv., 6 (2016) 10272–10279.
[39] A. Ausavasukhi, C. Kampoosaen, O. Kengnok, Adsorption characteristics of Congo red on carbonized leonardite, J. Clean. Prod., 134 (2016) 506–514.
[40] V.S. Munagapati, D.-S. Kim, Adsorption of anionic azo dye Congo Red from aqueous solution by cationic modified orange peel powder, J. Mol. Liq., 220 (2016) 540–548.
[41] X. Rong, F. Qiu, J. Qin, H. Zhao, J. Yan, D. Yang, A facile hydrothermal synthesis, adsorption kinetics and isotherms to Congo Red azo-dye from aqueous solution of NiO/graphene nanosheets adsorbent, J. Ind. Eng. Chem., 26 (2015) 354–363.
[42] K.-H. Goh, T.-T. Lim, Z. Dong, Application of layered double hydroxides for removal of oxyanions: a review, Water Res., 42 (2008) 1343–1368.